scientific reports

OPEN

First detection of industrial hydrogen emissions using high precision mobile measurements in ambient air

Iris M. Westra[1 ✉], Hubertus A. Scheeren[1], Firmin T. Stroo[1], Steven M. A. C. van Heuven[1], Bert A. M. Kers[1], Wouter Peters[1,2] & Harro A. J. Meijer[1]

Projections towards 2050 of the global hydrogen (H_2) demand indicate an eight-fold increase in present-day hydrogen consumption. Leakage during production, transport, and consumption therefore presents a large potential for increases in the atmospheric hydrogen burden. Although not a greenhouse gas itself, hydrogen has important indirect climate effects, and the Global Warming Potential of H_2 is estimated to be 12.8 times that of CO_2. Available technologies to detect hydrogen emissions have been targeted at risk mitigation of industrial facilities, while smaller climate-relevant emissions remain undetected. The latter requires measurement capacity at the parts-per-billion level (ppb). We developed and demonstrated an effective method to detect small hydrogen emissions from industrial installations that combines active AirCore sampling with ppb-precision analysis by gas chromatography. We applied our methodology at a chemical park in the province of Groningen, the Netherlands, where several hydrogen production and storage facilities are concentrated. From a car and an unmanned aerial vehicle, we detected and quantified for the first time small but persistent industrial emissions from leakage and purging across the hydrogen value chain, which include electrolysers, a hydrogen fuelling station, and chemical production plants. Our emission estimates indicate current loss rates up to 4.2% of the estimated production and storage in these facilities. This is sufficiently large to urgently flag the need for monitoring and verification of H_2 emissions for the purpose of understanding our climate change trajectory in the 21st century.

To achieve a zero or low-carbon energy economy, an energy carrier capable of zero emissions of air pollutants and greenhouse gases is needed. Molecular hydrogen (H_2) emerges as a promising contender for this role in this energy transition[13,31]. Initiatives such as the U.S. National Clean Hydrogen Strategy and Roadmap, Germany's 'Energiewende', and the hydrogen roadmap of the Netherlands ('Nationaal Waterstof Programma') alongside numerous other programs, underscore countries' ambitions towards a hydrogen value chain[9,20,24,39]. However, due to hydrogen's pivotal role in the energy transition, the expected increasing release of anthropogenic H_2 emissions into the atmosphere can result in enhanced global warming from indirect effects.

Increased levels of atmospheric H_2 can result in the lengthening of the lifetime of CH_4 and ozone, and higher levels of stratospheric water vapour[4,12,13,27,32,38,43,45]. Adding up to a global warming potential of 12.8 ± 5.2 over 100 years and a perturbation lifetime of 1.9 ± 0.5 years in the atmosphere, H_2 surpasses carbon dioxide (CO_2) in terms of greenhouse gas potency[12,14,25,41,42]. The current estimates of the loss rate potential (including venting, purging and uncontrolled leakage) of anthropogenic H_2 emissions, solely based on models, range from 1 to 10% of the total production[13,35]. So far, however, these estimates have not been validated at all by actual measurements, due to the lack of appropriate measurement techniques.

Currently, H_2 detectors utilised in industry are used for safety purposes only. Since the flammability range of H_2 is at 4% volume, handheld detectors with a detection limit starting at 30 μmol mol^{-1} or ppm up to 10% volume are used. However, since the atmospheric background concentration (mole fraction) of molecular hydrogen is ~0.5 ppm, anthropogenic H_2 from leakages with no flammability risk but a potential impact on the climate remains undetected. Precise atmospheric H_2 measurements within the scientific world started in 1957 with the introduction of the principle of liquefaction of air[11], followed in the 1970s[33] with a gas chromatographic

[1]Centre for Isotope Research (CIO), Energy and Sustainability Research Institute Groningen (ESRIG), University of Groningen, Nijenborgh 6, Groningen 9747 AG, The Netherlands. [2]Meteorology and Air Quality, Wageningen University and Research Center, Wageningen, The Netherlands. ✉email: i.m.westra@rug.nl

(GC) method, designed to analyse molecular hydrogen in atmospheric air based on the reduction of mercuric oxide. In 1994, Wentworth et al.[44] designed the pulsed discharge helium ionisation detector (PDHID), for use in a widespread range of applications outside atmospheric science. In 2009, Novelli et al.[23] adopted this method on a GC-system to measure molecular hydrogen in the atmosphere. The GC-PDHID technique showed a stable performance with a linear response over the 0-2000 nmol mol^{-1} or ppb range (AGAGE[30], CSIRO[8], NOAA[28,29]). The combination of this lab-based-measurement system with active AirCore sampling on mobile platforms, is the novel technique designed, tested and demonstrated in this study. The active AirCore is a long thin tube that can collect a profile of the trace gas of interest and preserve it during sampling, storage and analysis with minimum diffusive mixing[2,17]. The active AirCore was first designed and used for applications focused on CH_4 from the energy (e.g. coal mines[1]) and the agricultural sector (e.g. farms[40]). In our study, the application of the active AirCore sampling technique is broadened to also include the sampling and analysis of atmospheric H_2.

While the energy transition unrolls, further insights into the hydrogen value chain (production, transport, storage, end-use applications) and the potential risks of H_2 losses are of great importance[9,19,21,43]. Historically, studies like EUROHYDROS[45], Harvard Forest 1996–1998[3], Mace head 1994–1998[34], focused on the natural hydrogen budget through short-term campaigns. Long-established international networks (AGE-AGAGE, NOAA, more recently ICOS[29,30]) have been measuring atmospheric H_2 in an accurate and systematic way, but their stations are mostly remote. Until now, field campaigns specifically focused on regional and local anthropogenic H_2 emission sources originating from the hydrogen value chain have been absent. In Sun et al. (2024)[35] it is rightly pointed out that: *"It is important to note that the rates of hydrogen emissions are currently unknown across the value chain. Empirical measurements are needed to improve our understanding of where emissions are coming from and in what quantities."*. Consequently, to bridge the gap between model predictions and reality, our study offers innovative and versatile sampling techniques combined with a state-of-the-art high-precision hydrogen analysis system to provide empirical data from atmospheric H_2 mole fractions originating from industrial activities.

Our study is the first -to our knowledge- that provides such empirical measurements from atmospheric H_2 mole fractions originating from industrial activities. The proof of concept for this study entails detailed measurements of atmospheric H_2 using the active AirCore sampling technique at an industrial site in the province of Groningen (the Netherlands). We first outline our analysis and sampling techniques, after which we discuss the measurement site and necessary a priori information. We then present our observations from two mobile platforms (car and unmanned aerial vehicle (UAV)) before quantifying the emissions from the downwind sources. We use both a Mass Balance approach and an inverse Gaussian approach with multiple source configurations, and we discuss their respective uncertainties. We finish the paper with conclusions and a future outlook for our novel methodology.

Methods
Sampling methods
Active AirCore

The AirCore is an atmospheric sampling system that consists of a thin-wall stainless-steel (S.S.) tubing in the shape of a coil with a passivated inner surface, invented and patented by Pieter Tans[17]. The original design is used to obtain a vertical atmospheric profile by filling itself using the air pressure gradient in the atmosphere. Our "active" AirCore (length 245–285 m, $^3/_{16}$" OD) collects air samples via the use of a micro-pump (KNF NMP015 KPDC-B 6V) and a mass flow controller or a critical orifice to regulate the flow[2,36]. The AirCore is filled, through a chemical dryer using magnesium perchlorate located at the inlet of the system, with a dried profile of the trace gas of interest along a given measurement trajectory[2,36,37]. For our experiments, two AirCores were used. One was designed and described by Tong et al. (2023; for more details the reader is referred to this paper), the other is a simplified version thereof (see Supplementary Information (Sect. 1: Methods & Materials "*Road vehicle (passenger car) active AirCore system details*" & "*Unmanned Aerial Vehicle (UAV) active AirCore system details*"). These active AirCores were used on two mobile platforms: driven with a passenger car and flown with a UAV. For the passenger car, we used an active AirCore with a sample volume of 4.1 L. This AirCore is filled to a end-pressure of up to 1.6 bar over the course of about 2 hours of sampling, resulting in up to 38 useful discrete H_2 samples for the GC-PDHID (described in detail in Sect. 2.2). The sampling flow rate was constant and was set to either 45 or 60 ml min^{-1}, depending on the desired duration of the sampling. For the active AirCore applied on the UAV the maximum sample volume was 3.7 L. It was filled at atmospheric pressure with a flow of 200 ml min^{-1} over the course of about 15 minutes of flight time, allowing for up to 21 useful discrete H_2 samples. Prior to each field campaign, both AirCores were filled with synthetic air (UN1956; 20.5 Vol. % O_2, rest N_2), to clean the coil and identify a clear starting point of zero mole fraction H_2 during the analysis.

Flasks samples

As a complementary method to validate the AirCore H_2 measurements, vacuumized and dried 2.4 L glass flasks (with two Louwers Hapert Viton sealed valves) were filled at atmospheric pressure in pairs along the measurement trajectory. To obtain dry air samples, a magnesium perchlorate dryer tube was applied on the flask inlet. All mole fraction analyses of the glass flasks were conducted by both the GC-PDHID for H_2 and a cavity ringdown spectrometer (CRDS) system (Picarro Inc. CA, model G2401)[5,22] for mole fractions of CO_2, CH_4, and CO, the latter to get additional information on the potential emission sources co-located with H_2.

Analysis methods
GC-PDHID system

For the detection of molecular H_2 in the atmosphere we use an Agilent 8890 Gas Chromatograph (GC) equipped with a pulsed discharge helium ionisation detector (PDHID, Agilent) designed after Novelli et al. (2009). In

addition, our GC-system was fitted with a separate analysis line for N_2O and SF_6 equipped with a micro electron capture detector (μECD, Agilent) of which more details are given in the Supplementary information (Sect. 1: Methods & Materials " *The GC-PDHID system set-up*"). For the purpose of this paper, we will focus here on the PDHID analysis used for the detection of H_2. First, sample air is flushed over a 2 ml sample loop for H_2 (and 5 ml for N_2O/SF_6) at a rate of 52 ± 2 ml min^{-1} for 1.37 min. As such, the average sample size used for one measurement is 137 ± 5 ml which includes the overshoot of the pressure controller and the dead volume of the tubing and valves (using $\frac{1}{16}$" OD and 1/8" OD S.S. Swagelok) between the sample carrier (flask or AirCore) and the loops (2 ml & 5 ml). Secondly, for 30 s the sample loop is equilibrated from 1.5 bar filling pressure to ambient pressure (the exhaust of the loop is equipped with a 1 m x $\frac{1}{16}$" OD coil to prevent back-diffusion of lab air). Then, the sample is injected onto the first packed pre-column (Agilent S.S. packed column, 4.5 m x 1/8" OD x 2 mm, Hayesep-DB, 100–120 mesh) where H_2 is separated from the air matrix. Right after elution of the H_2 onto the second analytical column (Agilent S.S. packed column, 4.5 m x 1/8" OD x 2 mm, Hayesep-DB, 80–100 mesh), the pre-column is set into backflush mode to prevent oxygen and other contaminants from reaching the analytical column and detector. At 5.3 ± 0.3 min the H_2 peak reaches the detector, and it shows a 19.5 ± 1 s wide chromatogram. The total measurement time for one sample is 7 min. Potential drift is corrected by measuring a reference tank every 3 samples. Our GC-PDHID measures H_2 with a precision < 2 ppb and it is calibrated against a suite of in-house made dry whole-air working standards which themselves are calibrated against 3 primary standards linked to the international NOAA-H2-X1996 hydrogen scale (maintained by the Max Planck Institute for Biogeochemistry (MPI-BGC) Jena, Germany)[15,16]. The absolute accuracy of the primary standards is < 1 ppb. For more details about our GC-setup and measurement procedure, we refer to the Supplementary information (Sect. 1: Methods & Materials " *The GC-PDHID system set-up*").

AirCore analysis on the GC-PDHID
During analysis, the inlet of the active AirCore is connected to a push gas, while the outlet is connected to the sample inlet of the GC. As a push gas, the same H_2-free synthetic air as for the prefilling (at 1 bar over-pressure) was used, clearly marking the start and end of the atmospheric sampling sequence.

The GC-system uses an electronic pressure controller to regulate the flow. Typically, the push gas is set to the same pressure as the AirCore sample being around 1.6 bar absolute to minimise smearing of the sample. However, in our system, a slight overpressure of 0.4 bar is required to push the sample through our sample loop. Potential drift is corrected for by utilising a bracketing method, wherein up to 3 samples are bracketed by a known low and high standard for calibration. It should be noted that measurement uncertainty cannot be minimised by repetition or duplication, since by the very nature of the AirCore sampling technique, it is considered a series of unique samples.

AirCore sample storage time, sample resolution and positioning
The accuracy and precision of the active AirCore samples are dependent on the storage time following the completion of the field campaign. An AirCore sample is typically measured in the lab directly after a field campaign, to keep the storage time, and thus the smearing effects by molecular diffusion, as short as possible. Extensive laboratory storage tests were done to evaluate the profile loss, i.e. the storability of molecular hydrogen in an active AirCore and determine the necessary maximum time for which an accurate retrieval can be guaranteed. Further details regarding these experiments are available in the Supplementary information (Sect. 1: Methods & Materials "*Active AirCore sample storage and resolution tests*"). Across all sampling days, the median storage time, calculated from the ending of the sampling time, was for the car AirCore 0.75 h while for the UAV AirCore it was 1.41 h, before we started our analysis. For more information see the Supplementary information (Sect. 1: Methods & Materials "*Storage time of our car and UAV active AirCore samples*").

Given the continuous air sampling in the AirCore but discrete analyses on the GC, a relation needs to be established between the H_2 mole fractions and the path driven or flown. The spatial distribution is primarily influenced by sample size, sampling flow and mobility. With a constant sampling flow, each discrete sample linearly corresponds to a specific time duration and range of GPS coordinates. Smaller sample sizes increase the resolution of the trace gas profile and decrease the spatial distribution. Considering the spatial distribution, the samples are categorised into stationary and mobile, depending on whether the mobile platform (passenger car or UAV) was stationary or in motion. The analysis of the stationary samples is straightforward, the GPS-coordinates directly pinpoint the representative location. The mobile samples require additional interpretation and assumptions. As the mobile platform (passenger car or UAV) moves during sampling, each discrete sample corresponds to a range of GPS-coordinates. Given the filling mode of the sample loop (see 2.2.1), the actual sampled air of the discrete sample corresponds to the final segment of the loop flush. The assigned location is deducted to be at $83 \pm 10\%$ of the discrete sample's transect, based on the loss during equilibration and the flushing time, a more extensive explanation is given in the Supplementary information (Sect. 1: Methods & Materials "*Car active AirCore 2-D spatial distribution of a discrete sample*" and "*UAV active AirCore 2-D spatial distribution of a discrete sample*").

Flasks analysis
The flasks filled in the field were measured on the GC-PDHID for H_2 and on the CRDS system for CO_2, CO and CH_4 with well-established methods in our lab[22], more details in the Supplementary information (Sect. 1: Methods & Materials "*Flask analysis of H_2 on the GC-PDHID*" and "*Flask analysis of CO_2, CH_4, and CO on the CRDS-system*").
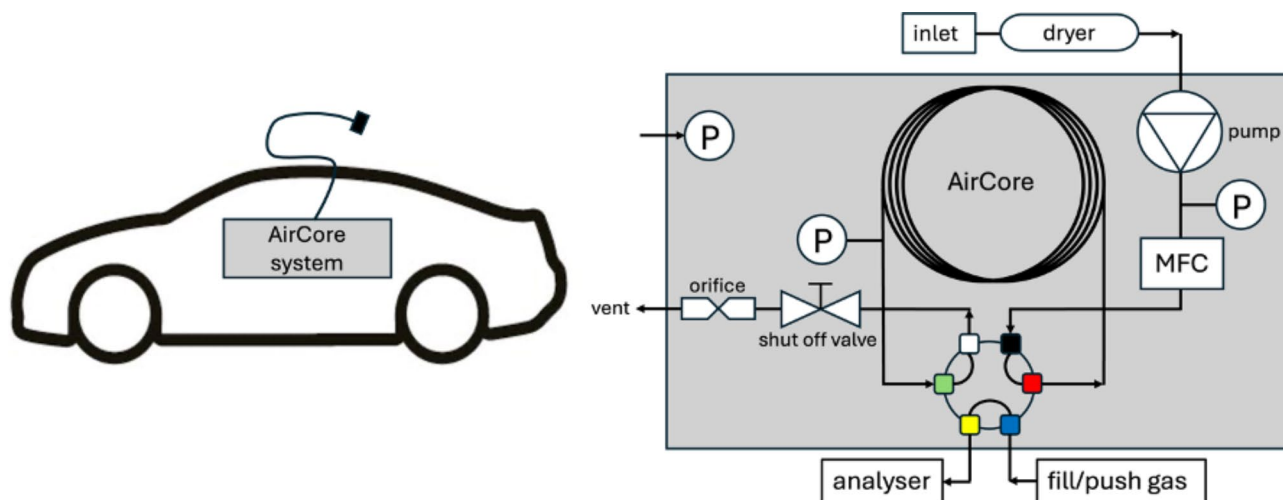
Fig. 1. For sampling from a passenger car, the active AirCore is positioned at the backseat, as indicated by the black box, with the inlet outside of the window. The active AirCore is set to the sampling & calibration mode, making the sampled air enter via the inlet. P presents the pressure controller and MFC stands for mass flow controller.
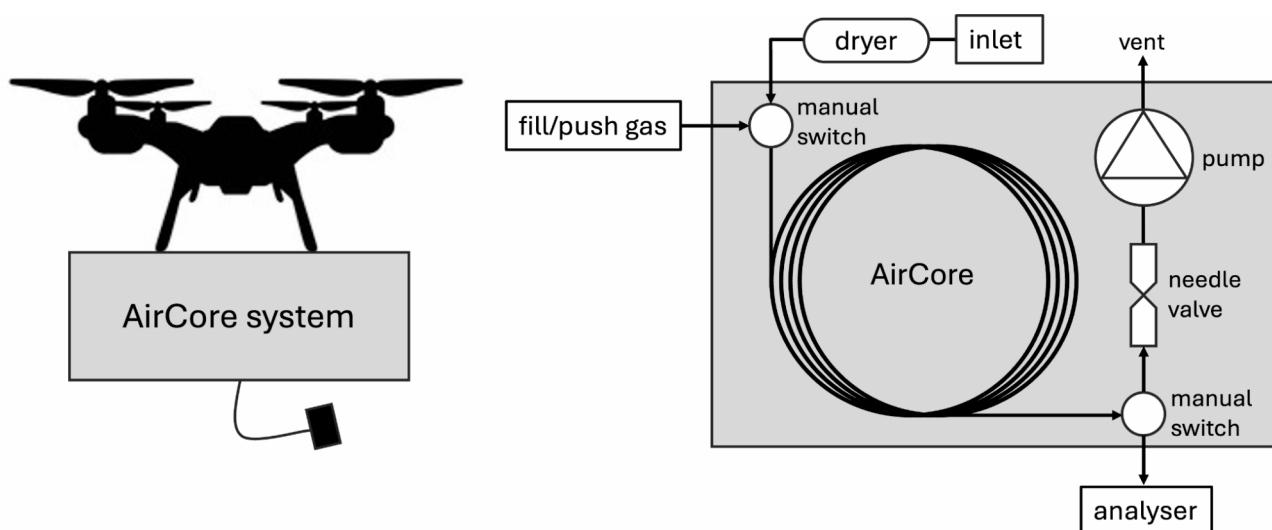

Fig. 2. For the mobile platform, UAV, the active AirCore is positioned at the bottom of the UAV, as indicated by the black box. On the right of the figure the schematic representation of the UAV AirCore is shown.

Measurement platforms

Passenger car   For sampling from a passenger car, the sampler is installed on the backseat next to the operator. The inlet of the AirCore is positioned outside of the car's rear window (Fig. 1) with the filter facing backwards and downwards to protect the inlet from potential rainfall and impact from insects. The measurement starts when the AirCore is set to sampling mode and the pump flow is set to either 45 or 60 ml min^{-1}. A detailed description of the car AirCore is provided in the Supplementary information (Sect. 1: Methods & Materials "*Road vehicle (passenger car) active AirCore system details*"). The ambient air is dried at the inlet of the AirCore with magnesium perchlorate. The active AirCore in the passenger car is equipped with a GPS tracker and a logger for timestamp, pump pressure, coil pressure, volume sampled, and volume collected in the coil. Directly after the sampling is completed (typically 2 h duration) the AirCore is transported back to the laboratory for analysis.

Unmanned aerial vehicle (UAV)   The used UAV (DJI Matrice 600) or drone has a payload capacity of 6 kg, just sufficient for our Active AirCore system with a mass of 6 kg. Considering the AirCore's volume, the flow rate was set to fill the AirCore to 80% during the maximum flight duration of 15 min. Flight restrictions limited the vertical profile to a maximum altitude of 140 m. The UAV AirCore system is a simplified variant of the car version, with a manual pull (not push) pump and switch and without data logging. The GPS tracking, flight speed, altitude, and other technical parameters are recorded by the UAV. Figure 2 shows a schematic of the UAV AirCore
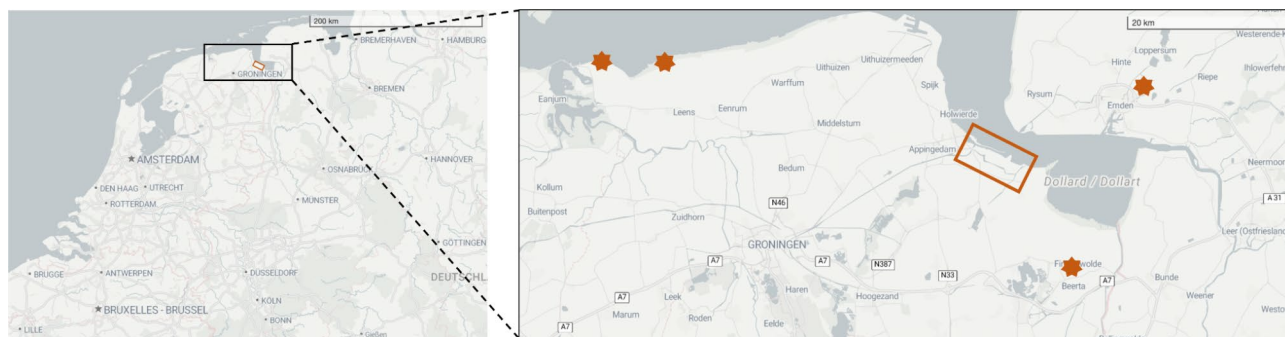
Fig. 3. The orange stars in the right-hand-side figure indicate (from left to right) the meteorological stations Lauwersoog (the Netherlands), Lutjewad (the Netherlands), Nieuw-Beerta (the Netherlands) and Emden (Germany). The orange rectangle represents the Chemical Park Delfzijl (map by using Rstudio, Leaflet).

Date (dd-mm-yy)	Production per day (10^7 g)	Emission per day (10^3 g)
04-08-23	2.05 ± 0.33	730 ± 70
06-09-23 to 20-12-23	2.05 ± 0.33	8.3 ± 0.8

Table 1. Production and emission estimates, as provided via personal communication.

setup, for more details we refer to the Supplementary information (Sect. 1: Methods & Materials "*Unmanned Aerial Vehicle (UAV) active AirCore system details*").

Measurement site

Site description
Located on the northeastern side of Groningen (the Netherlands), the Chemical Park Delfzijl (53.3105 N, 6.9752 E) (Fig. 3) offers an ideal site for the field campaigns outlined for this study. With the Wadden Sea located to the north of the park and rural areas extending at least 18 km southward (SLD: Straight-line distance), minimal external influences on the atmospheric H_2 mole fractions are ensured. The chemical park is a confined property (approx. 4 km²) surrounded by a rural environment with large-scale and fully operational chemical industry in which molecular hydrogen is either produced, transported, stored or consumed within the park. Predominantly during northwesterly winds, the emissions from the park itself were easily distinguishable downwind of the park, while easterly winds allowed for observing background conditions from the surrounding agricultural area. The closest potential polluter outside of the park is the seaport Eemshaven, 17 km SLD away to the northwest, hosting coal-and gas-fired power plants but so-far no known H_2-emitting processes. Towards the west-southwest at 28 km SLD a potential H_2 emitter is the urban area of the city of Groningen, with e.g. a H_2 fuelling station and H_2 buses. The good accessibility of Chemical Park Delfzijl, without the need for permits or registration for all mobile platforms, facilitated the field campaigns. Furthermore, the cooperation with the industry stakeholders strengthens the eventual emission and loss rate estimates, because of the specifications given on the processes and production rates (through personal communication). Considering the sampling equipment, the proximity of Delfzijl to our laboratory ensured the profile accuracy by maintaining minimum storage times. Even though the primary processes in the chemical park in Delfzijl are not entirely representative of the complete hydrogen value chain, it is crucial to identify potential H_2 losses from real facilities, before a widespread implementation is completed.

Industrial hydrogen production and emission estimates
For our purpose, the Chemical Park Delfzijl houses four relevant industries, based on a priori information about production and emission processes, to ensure confidentiality the industries in question will be referred to by an arbitrary numbering. At industry N1 (Industry N1 consists of two processes), NaOH, Cl and H_2 are produced from brine via the process of electrolysis (1a). The surplus H_2 is transported over the park to a nearby power plant for combustion (1b) and to industry F3 for direct usage at a hydrogen fuelling station. Any remaining H_2 is directly vented. At industry E2 hydrogen peroxide is produced, for which in-house H_2 is produced from steam-methane reformation.

For industries N1 and E2, hydrogen emissions from purging and venting on sampling days are known (personal communication). Since no emission data for F3 are available, a loss rate estimation of 0.5% ($\sim 0.24\%$ high-pressure storage, $\sim 0.25\%$ compressor leakage) is used from the known storage present[9]. Industry R4 encompasses all remaining factories/companies for which no a priori information is available regarding H_2 production, consumption, purging or venting. The daily production is calculated using the average annual production rate for industry N1 and industry E2. Combined with the H_2 consumption of industry F3, the estimated production and emission rates per day are summarised in Table 1, where only for day 1 the H_2 emissions differ from the rest of the measurement days. A detailed description of the daily production and

emission estimates per category is provided in the Supplementary information (Sect. 1: Methods & Materials *"Daily H$_2$production and emission rates from the Chemical Park Delfzijl"*).

Emission estimate methods and uncertainties

Mass Balance approach

We apply a Mass Balance approach to estimate the amount of H$_2$ emitted in g s^{-1} by the Chemical Park Delfzijl industries, by using the enhancement of atmospheric H$_2$ in an assumedly homogenous distributed 2D plane downwind of the park[1,7,18,26,36]. We use the following simple Mass Balance equation to derive the H$_2$ flux (Q in g s^{-1}) across the transect within the downwind plane of the chemical park:

$$Q = C \cdot \frac{\overline{u} \cdot \cos(\theta) \cdot \Delta A \cdot M_{H2} \cdot P}{R \cdot T} \tag{1}$$

In the Mass Balance Eq. (1), C is the enhancement of the H$_2$ mole fraction [mol H$_2$/mol air] over background values. The average wind speed is denoted by ū [m s^{-1}], and the area of a vertical grid box perpendicular to the wind direction is given by ΔA [m^2]. The daily values (Table S4) and derivation of wind speed and direction are given in the Supplementary information (Sect. 1: Methods & Materials *"Estimating emissions: The Mass Balance approach"*). To account for uncertainty in the mean wind direction, a deviation to the wind angle (assumed perpendicular to the grid box) is represented by θ [degrees]. Finally, the molar mass of H$_2$ is given by M$_{H2}$, P is the air pressure [Pa], R is the universal gas constant [m^3·Pa·K^{-1}·mol^{-1}] and T is the mean atmospheric temperature [K]. We assume a standard atmospheric air pressure of 101325 Pa and an air temperature of 288.15 K.

We applied the Mass Balance approach using a Monte Carlo approach (*N* = 500 simulations) to account for parameter uncertainties. Our simulations include uncertainties related to wind speed, wind direction, plume width, and plume height[10]. Detailed descriptions of the determination and quantification of these uncertainties can be found in the Supplementary Information (Sect. 1: Methods & Materials, *"Estimating Emissions: The Mass Balance Approach"*).

Inverse gaussian dispersion model approach

We also derive emission rates using the inverse Gaussian approach as a control and substantiation to the Mass Balance approach. For this, we used a standard point source Gaussian dispersion model (Eq. (2)) in combination with the three-dimensional mole fraction data from the active AirCore measurements.

$$C(x,y,z) = \frac{Q}{2\pi \, \sigma_y(x) \, \sigma_z(x) \, \overline{u}} exp\left(-\frac{(y-y_s)^2}{2\sigma_y^2(x)}\right)\left[exp\left(\frac{(z-z_s^2)}{2\sigma_z^2(x)}\right) + exp\left(\frac{(z+z_s^2)}{2\sigma_z^2(x)}\right)\right] \tag{2}$$

In the Gaussian dispersion model, C(x, y, z) are the enhanced H$_2$ mole fractions [mol H$_2$ mol air^{-1}] inside the plume at specific coordinates (x, y, z in metres) downwind from a source in the Chemical Park Delfzijl. Q is the emission rate in [g s^{-1}] and ū is the mean wind speed along the plume direction in [m s^{-1}]. We use the same values as the Mass Balance approach for wind speed and wind direction. The stability parameters and with units [m] (Eq. (3)) describe horizontal and vertical mixing. They depend on atmospheric stability and can be calculated using the Pasquill Gifford parameters. The last exponential term in the equation represents the reflection of plumes from the surface[6].

$$\sigma_y = \frac{r \cdot x}{(1+\frac{x}{a})^P} \quad \sigma_z = \frac{s \cdot x}{(1+\frac{x}{a})^q} \tag{3}$$

We identify 5 point sources for H$_2$ in the Chemical Park Delfzijl that can be linked to activities involving significant production, storage or usage of H$_2$ (see Sect. 2.3.2). Point source locations (surface coordinates and emission height) are chosen based on process type and personal communication.

We also applied the inverse Gaussian approach using a Monte Carlo approach (*N* = 500 simulations) to account for parameter uncertainties and to ensure not only local minima are found. Our simulations capture uncertainties related to wind speed, wind direction, atmospheric stability, measurement errors and emission height. Detailed descriptions of the determination and quantification of these uncertainties can be found in the Supplementary Information (Sect. 1: Methods & Materials, *"Estimating Emissions: The inverse Gaussian plume model approach"*).

Field campaigns

A total of 7 sampling transects on 7 separate days have been made with the active AirCore system aboard the passenger car. For 3 out of 7 transects driven on 4th August, 11th September and 6th December, in the afternoon between 14:00 (HH: MM) and 16:00 local time (LT), the wind direction spanned west to north (270–350 degrees), as shown in Fig. 4. Four UAV flights were performed, three of them lasting between 10 and 13 min and were carried out on 5th, 12th, 17th October. The fourth transect was flown on the 6th December of 2023 in the afternoon between 14:00 and 16:00 LT. In total three transects were flown successfully downwind and one upwind of the chemical park. The height of the vertical profiles spans from 0 m (ground level) to ~ 140 m in altitude. Both the passenger car and UAV flight details are summarised in the Supplementary information (Sect. 1: Results and Discussion *"Overview of field campaigns"*).
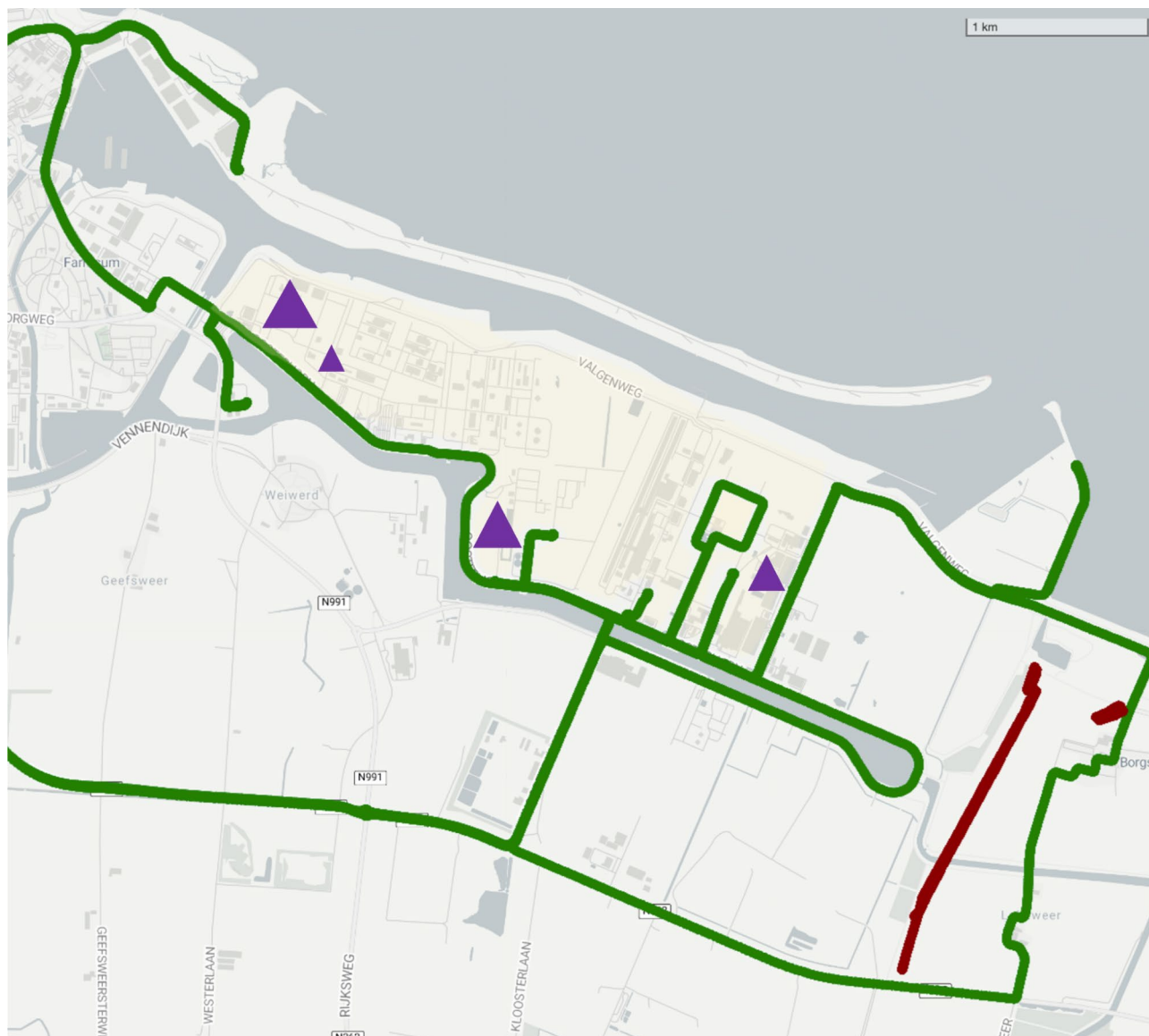
Fig. 4. The Chemical Park Delfzijl is highlighted in yellow with the purple triangles indicating the H_2-related industry. The summary of all trajectories driven with the passenger car were plotted along the green trajectories and in darkred the trajectories flown with the UAV.

Results & discussion

Active AirCore passenger car results

We measured strong enhancements of H_2 mole fractions with values up to 1346 ± 2 ppb downwind of the chemical park, relative to 530 ± 11 ppb upwind. We summarise this data in Fig. 5 with a 3D visualisation of individual samples' enhancement over the background, displayed along the northwesterly angle of incidence, corresponding to the wind direction. Out of 53 downwind samples analysed, 35 (66%) had > 100 ppb enhancements, a number that is much larger than the typical seasonal changes, trends, and enhancements found at long-term monitoring sites that are situated away from local sources[29]. With no atmospheric chemical pathway to produce this hydrogen in-situ, this unequivocally points towards substantial emissions of H_2 in the Delfzijl park.

These emissions are not incidental but systematic (Fig. 6), as we find them across all sampling days and also under different wind directions and atmospheric conditions. Compared to the samples collected upwind of the park, the downwind data shows consistently enhanced atmospheric H_2 mole fractions, averaging 30 up to 280 ppb each day. Furthermore, likely due to an inhomogeneous release of anthropogenic H_2 emissions from the chemical park, there is high variability (± 92 ppb) in the enhancement of individual samples collected on the same day. In contrast, the upwind sampled data remains consistently close to the atmospheric background mole fraction of H_2 (532 ± 6 ppb). Moreover, the very low variability (1σ standard deviation) of the upwind data
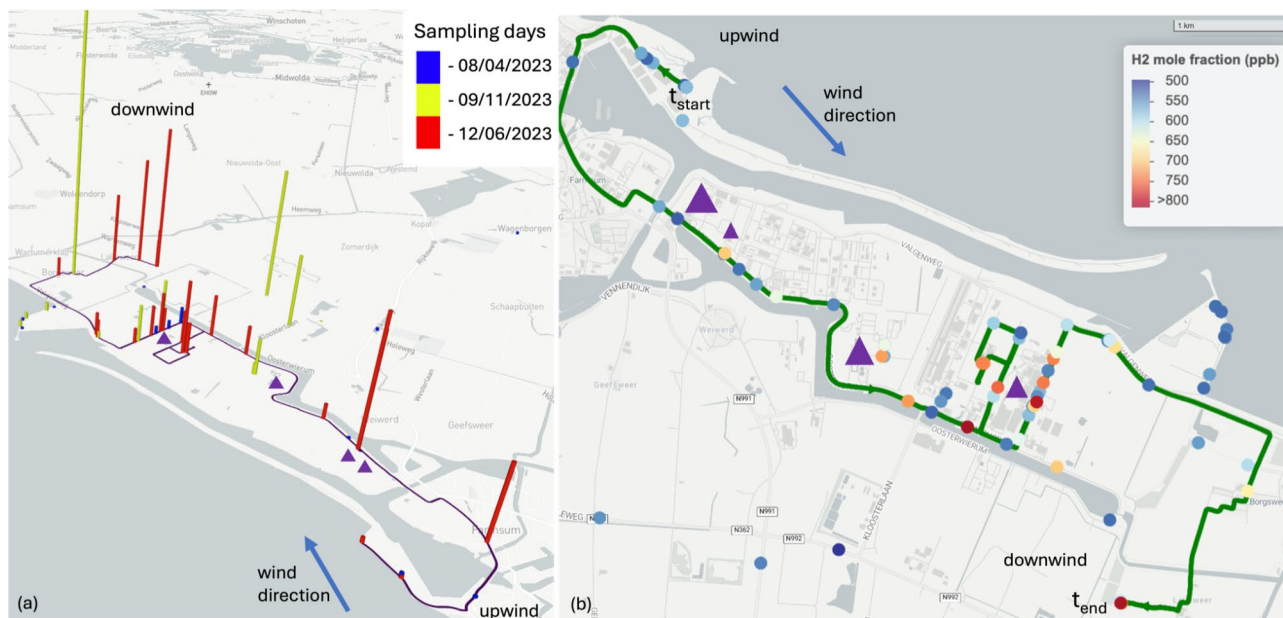
Fig. 5. Summary of the atmospheric H_2 mole fraction obtained with the passenger car along the main trajectory along the park from NW wind direction, indicated by the blue arrow with the purple triangles indicating molecular hydrogen-related industry. (a) The colour of the columns indicates the sampling day, and the height of the column indicates the relative atmospheric H_2 mole fraction to the background. (b) Data points represent the atmospheric H_2 mole fractions distributed over the park. The size of the purple triangle roughly indicates the size of the H_2 activity relative to the total at the chemical park.
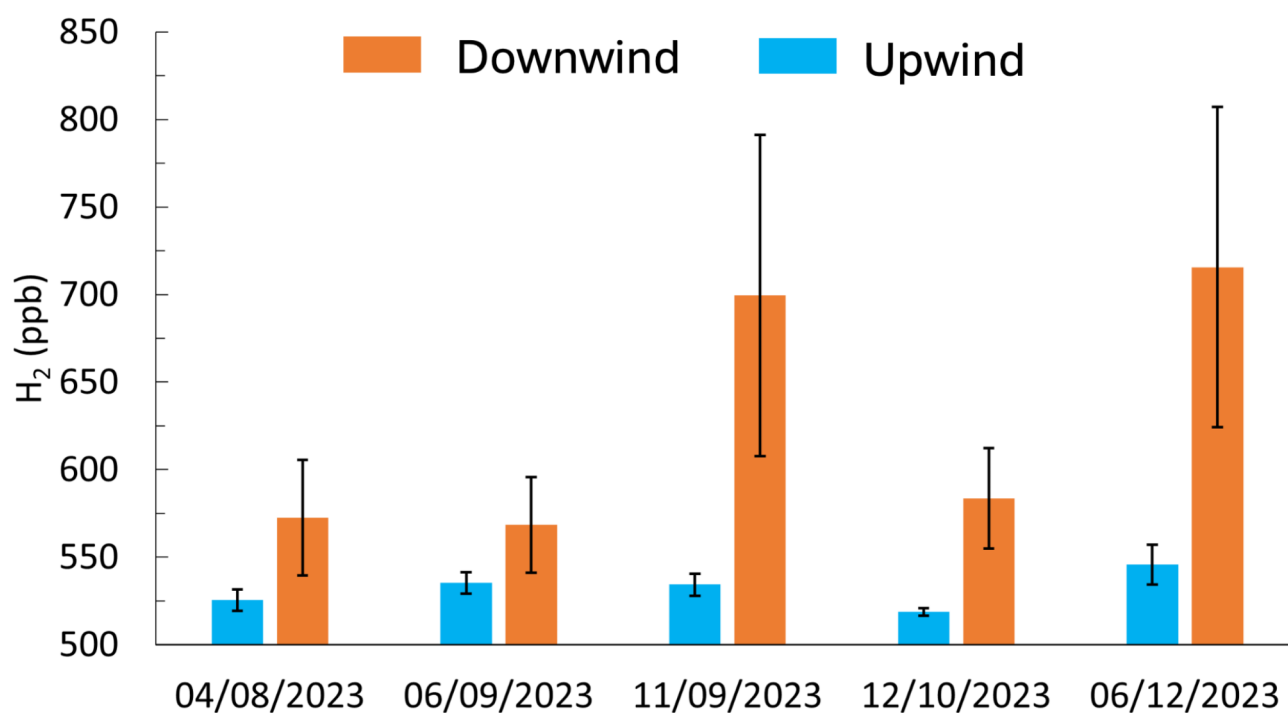
Fig. 6. The median atmospheric H_2 mole fraction for each sampling day categorised by upwind (blue) and downwind (orange). On the x-axis, the date is shown with on the y-axis the atmospheric H_2 mole fraction (ppb). The error bars denote the measurement variability given by the 1σ standard deviation.

emphasises the stability of the atmospheric background mole fraction as well as that of our sampling and analysis system, as expected when no nearby sources have influenced the samples.

Active AirCore UAV results

UAV-based sampling confirmed the existence of substantial H_2 sources in the Chemical park Delfzijl, although downwind measured mole fraction enhancements at the vertical flight heights of the UAV were lower (40–100 ppb of H_2) than we measured at the surface with the passenger car. The relatively low 1σ standard deviation ± 35 ppb for all downwind flight data points, relative to the car results (Fig. 6), indicates a well-mixed H_2 plume. Figure 7 summarises the comparison of two enhanced downwind sampling profiles with a background upwind vertical profile. Even though the two downwind vertical profiles were not able to capture the top of the plume, the vertical profiles do show that H_2 for all measurement days was relatively well mixed vertically, and the average enhancements over the background exceeded the vertical H_2 gradients and variability. Local wind-shear effects near the surface could possibly have impacted data points below 20 m in both downwind profiles; such near-surface effects would also contribute to the higher variability found for our car samples.

Flasks sampling results

Our flask-derived data confirms the variability in enhanced H_2 mole fractions found at the Chemical Park Delfzijl. The H_2 mole fraction measured from the car and in the flasks for similar GPS-coordinates show for upwind locations a clear background signal while over the span of the park enhanced H_2 mole fractions up to 950 ppb were found, see the Supplementary information for more details (Sect. 2: Results & Discussion "*Flask sampling results for H_2*").

Next to this, our flask-derived data gives insight into co-located GHG emissions associated with atmospheric H_2 for three categories at the park: chemical processes from industry, microbial processes from biomass, and puff emissions from a hydrogen fuelling station. From Fig. 8, it is evident that general chemical processes from industry exhibit no clear co-location with CO and CH_4. Furthermore, the most enhanced atmospheric H_2 mole fractions, with no co-located GHGs, originate from the hydrogen fuelling station situated at the start of the park. Only at the rear of the park, near the biomass waste incinerator, a clear co-location between atmospheric H_2 and microbial processes was found based on observations of CO and CH_4.
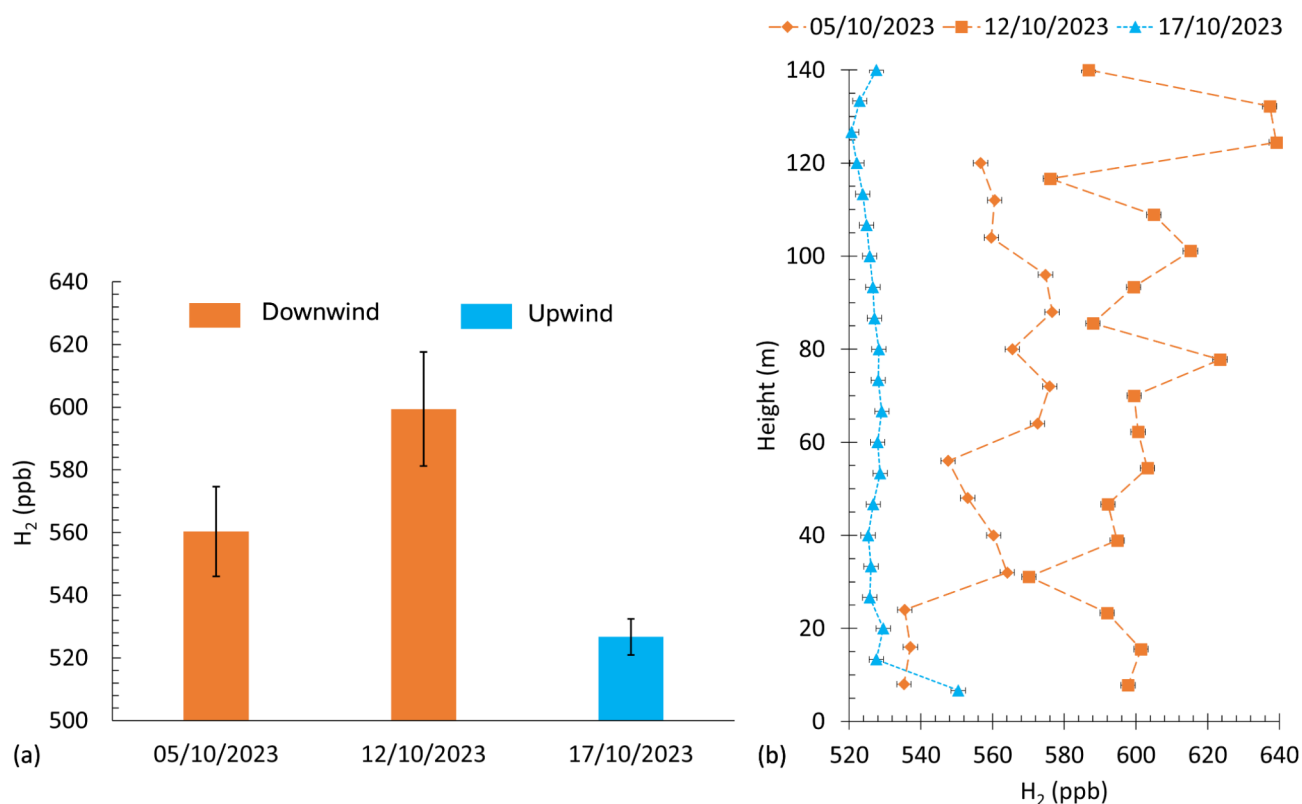
Fig. 7. The median atmospheric H_2 mole fraction for each sampling day is categorised by upwind (blue; no park contamination) and downwind (orange). (**a**) On the x-axis the date is shown with on the y-axis the atmospheric H_2 mole fraction (ppb). The error bars denote the measurement variability given by the 1σ standard deviation. For (**b**) three vertical profiles are shown, with the height in metres on the y-axis and the atmospheric H_2 mole fraction (ppb) on the x-axis. The error bars denote the measurement precision.
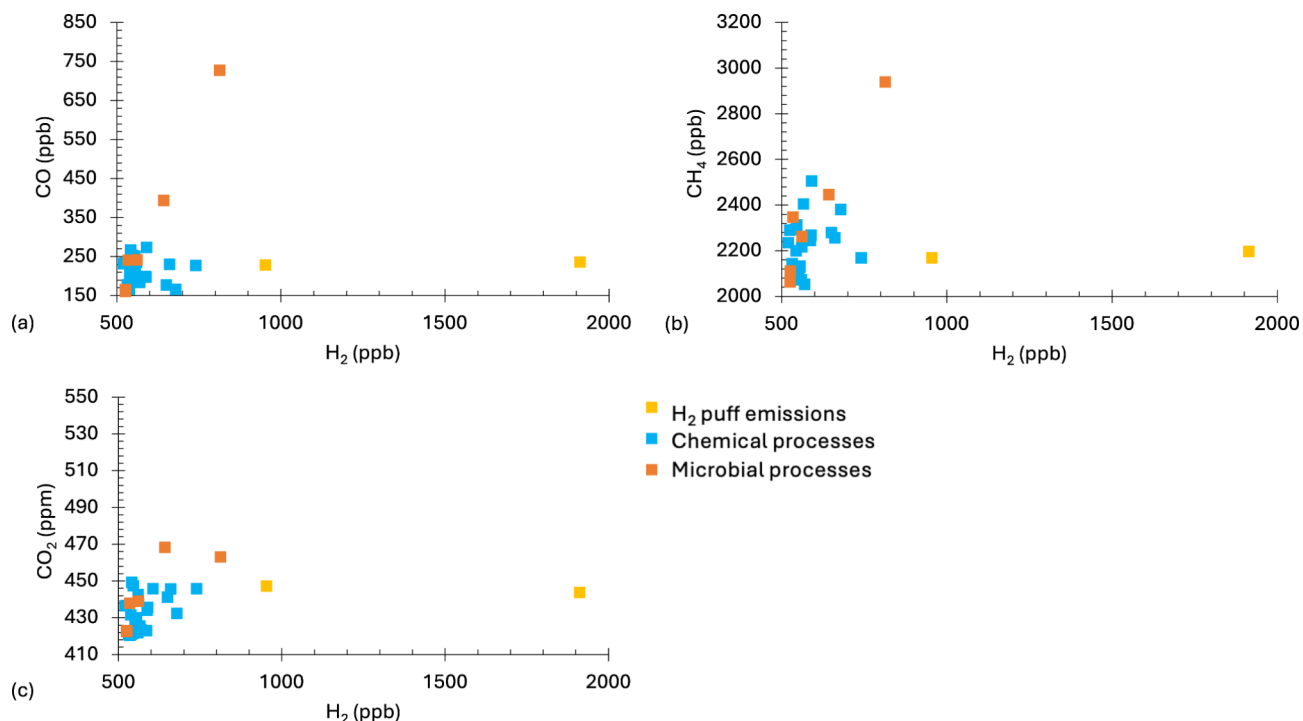
Fig. 8. The summary of the results obtained from the flask data is categorised based on location into H_2 puff emissions (yellow), chemical processes (blue) and microbial processes (orange). The x-axis displays the H_2 mole fraction (ppb) with the (**a**) CO (ppb), (**b**) CH_4 (ppb) and (**c**) CO_2 (ppm) on the y-axis.
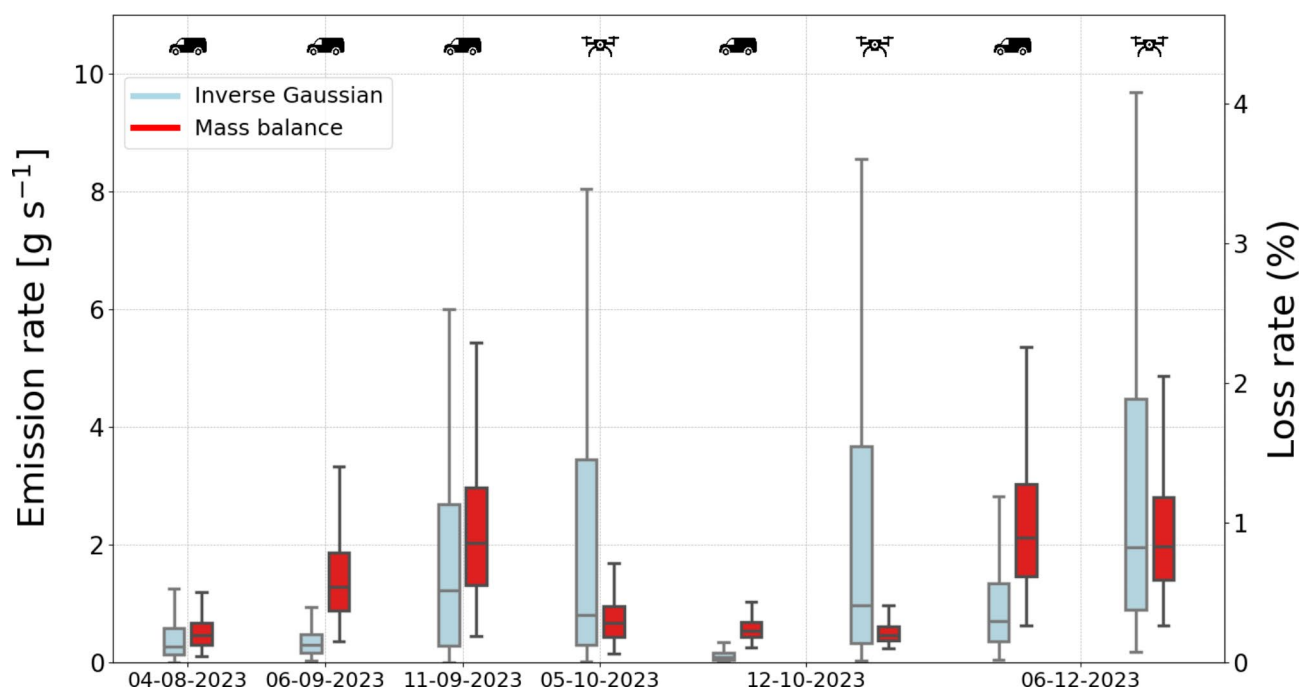
Fig. 9. Emission rate estimates and calculated loss rate for H_2 mole fraction from the inverse Gaussian and Mass Balance approach. Boxplots show the distribution of solutions for each day and data type (car or UAV). Boxes cover the first (Q1) to the third (Q3) quartile of solutions, with the median (Q2) solution in between. The whiskers extend to the rest of the data (except outliers). We define outliers as data points more than 1.5 times the interquartile range (IQR) below Q1 or above Q3. These are not shown to improve readability.

Emission estimates

We find loss rates (Fig. 9) up to 4.2% for H_2-related activities at the Chemical Park Delfzijl, relative to estimated daily production. On a day-to-day basis we find variations in emission rates originating from measured mole fractions and meteorological conditions, with median values ranging from 0.5 to 2.1 g s^{-1} (Mass Balance approach) to 0.1–2.0 g s^{-1} (inverse Gaussian approach).

The distributions presented in Fig. 9 also include the parameter uncertainty ranges discussed in Sect. 2.4, which are primarily related to meteorological conditions. The variation in the enhanced H_2 mole fraction suggests consistent but not uniform emissions over time, leading to diverse emission estimates. Furthermore, the relative homogeneity of the UAV-based profiles substantiates the continuous wide spread of emissions.

On the days when both car and UAV enhancements were sampled and measured, the emission estimates for the Mass Balance approach were highly similar. Also, we find a good agreement for all car data between the inverse Gaussian and Mass Balance approaches. We find the largest discrepancy between the inverse Gaussian and Mass Balance for the UAV-based estimates due to the large distance to sources combined with the higher sensitivity to wind direction for the former approach.

On average, the Mass Balance approach yields median emission rates 2.3 times as high as the inverse Gaussian approach on all days. This discrepancy is likely caused by the presence of high mole fraction samples near emission sources, which in the Mass Balance approach causes an overestimation of emissions due to an unrealistically large grid box area given the proximity to the source and the resulting short mixing time. In contrast, the Inverse Gaussian approach can explain these samples with lower emission rates, given the proximity to the source. The similarity between the loss rates determined from the UAV-based data and the car-based data enhances the robustness of the outcome.

Conclusions & Outlook

We developed a measurement method for low-level in-situ (semi)-continuous (industrial) H_2 emissions using an active AirCore sampler and a GC-PDHID analysis system. During a number of field campaigns significantly enhanced atmospheric H_2 mole fractions were detected at the industrial chemical park in Delfzijl (Groningen province, the Netherlands), ranging from downwind mole fractions of 580 ppb up to 1500 ppb. The consistency in the enhanced atmospheric H_2 mole fraction during every experiment indicated a continuity in H_2 emissions from the chemical park. In addition to the AirCore samples, we analysed grab samples from flasks collected during the field campaigns. These flasks were intercompared on H_2 with the AirCore data (at similar GPS-coordinates), and besides H_2, analysed on mole fractions of CO_2, CH_4, and CO to gather additional information on co-located processes. From the flask data, the enhanced H_2 mole fractions found at the chemical park could be divided into three sections: microbial production, chemical production and H_2 purge emissions. The flask results indicated that most of the enhanced H_2 mole fractions substantiated the AirCore data and did not correlate with enhanced mole fractions of CO_2, CO and CH_4 except for CH_4 and CO emissions in the proximity of a biomass waste incinerator at the park. The UAV-based AirCore downwind vertical profiles were relatively well mixed showing some plume variability in H_2 mole fraction along the 140 m altitude. The background upwind profile showed a nearly constant continuous background signal throughout the profile. Our first empirically determined emission estimates showed percentages (up to 4.2%) well within the range of model predictions. Our results represent a stepping stone in the development of an easy-to-use and highly accurate sampling technique to detect and quantify in situ H_2 emissions from leakage, purging and storage, pivotal for the development of the energy transition.

With the data obtained from this study, we hope to inform industry and policy makers to not oversee the environmental impact of current small H_2 emissions, considering the plans for significant upscaling of sectors along the hydrogen value chain. For future work, data gathered with our sampling and analysis method has the potential to substantiate model emission estimates across the hydrogen value chain. The methodology can be improved by minimising the sample size requirement of the GC, including additional in-situ meteorological measurements, and applying a new GC technique which is able to obtain simultaneous H_2, CO_2 and CH_4 for source characterization. Further work will focus on expanding and improving data sets along other parts of the hydrogen value chain.

Data availability

All data and analysis software used in this manuscript is accessible from an open access data archive under 'https://github.com/IrisMWestra/Atmospheric-hydrogen-Delfzijl-.git'. For more information correspondence should be addressed to I.M.W.

References

1. Andersen, T. *Quantifying Local to Regional Emissions of Methane Using UAV-based Atmospheric Concentration Measurements*. [Thesis fully internal (DIV), University of Groningen]. University of Groningen. https://doi.org/10.33612/diss.190478126 (2021).
2. Andersen, T., Scheeren, B., Peters, W. & Chen, H. A UAV-based active AirCore system for measurements of greenhouse gases. *Atmos. Meas. Tech.* **11**(5), 2683–2699. https://doi.org/10.5194/amt-11-2683-2018 (2018).
3. Barnes, D. H. et al. Hydrogen in the atmosphere: observations above a forest canopy in a polluted environment. *J. Geophys. Research: Atmos.* **108**(6). https://doi.org/10.1029/2001jd001199 (2003).
4. Bertagni, M. B., Pacala, S. W., Paulot, F. & Porporato, A. Risk of the hydrogen economy for atmospheric methane. *Nat. Commun.* **13**(1), 7706. https://doi.org/10.1038/s41467-022-35419-7 (2022).

5. Crosson, E. R. A cavity ring-down analyzer for measuring atmospheric levels of methane, carbon dioxide, and water vapor. *Appl. Phys. B: Lasers Opt.* 403–408. https://doi.org/10.1007/s00340-008-3135-y (2008). 92(3 SPECIAL ISSUE).

6. Csanady, G. T. *Turbulent Diffusion in the Environment*, Vol. 3. (D. Reidel Pub. Co., Boston, 1973).

7. Fiehn, A. et al. Estimating CH_4, CO_2 and CO emissions from coal mining and industrial activities in the Upper Silesian Coal Basin using an aircraft-based mass balance approach. *Atmos. Chem. Phys.* **20**(21), 12675–12695. https://doi.org/10.5194/acp-20-12675-2020 (2020).

8. Francey, R. J. et al. (Australia) measurement of greenhouse gases in the global atmosphere. In *Bureau of Meteorology and CSIRO Atmospheric Research*(eds Tindale, N. W., Derek, N. & Fraser, P. J.) 42–53 (Baseline Atmospheric Program Australia, Melbourne, 2003) http://hdl.handle.net/102.100.100/191835?index=1.

9. Frazer-Nash Consultancy. Fugitive hydrogen emissions in a future hydrogen economy. 52. (2022). FNC 012865-53172R (Issue 1)

10. Gerbig, C., Körner, S. & Lin, J. C. Vertical mixing in atmospheric tracer transport models: error characterization and propagation. *Atmos. Chem. Phys.* **8**, 591–602. https://doi.org/10.5194/acp-8-591-2008 (2008).

11. Glueckauf, E. & Kitt, G. P. The hydrogen content of atmospheric air at ground level. *Q. J. R. Meteorol. Soc.* **83**(358), 522–528. https://doi.org/10.1002/qj.49708335808 (1957).

12. Hauglustaine, D.: The climate impact of a future hydrogen economy, EGU General Assembly 2024, Vienna, Austria, 14–19 Apr 2024, EGU24-11016. https://doi.org/10.5194/egusphere-egu24-11016 (2024)

13. Hauglustaine, D. et al. Climate benefit of a future hydrogen economy. *Commun. Earth Environ.* **3**(1). https://doi.org/10.1038/s43247-022-00626-z (2022).

14. IPCC. *CLIMATE CHANGE 2001*(THE SCIENTIFIC BASIS, 2001).

15. GAW Report #194: 15th WMO/IAEA Meeting on Carbon Dioxide, Other Greenhouse Gases and Related Tracer Measurement Techniques, Jena, Germany, 7–10 September 2009 https://library.wmo.int/idurl/4/58718 (2011).

16. Jordan, A. & Steinberg, B. Calibration of atmospheric hydrogen measurements. *Atmos. Meas. Tech.* **4**(3), 509–521. https://doi.org/10.5194/amt-4-509-2011 (2011).

17. Karion, A., Sweeney, C., Tans, P. & Newberger, T. AirCore: an innovative atmospheric sampling system. *J. Atmos. Ocean. Technol.* **27**(11), 1839–1853. https://doi.org/10.1175/2010JTECHA1448.1 (2010).

18. Klausner, T. et al. Urban greenhouse gas emissions from the Berlin area: a case study using airborne CO_2 and CH_4 in situ observations in summer 2018. *Elementa*. **8**(1). https://doi.org/10.1525/ELEMENTA.411 (2020).

19. Lipiäinen, S., Lipiäinen, K., Ahola, A. & Vakkilainen, E. Use of existing gas infrastructure in European hydrogen economy. *Int. J. Hydrog. Energy*. **48**(80), 31317–31329. https://doi.org/10.1016/j.ijhydene.2023.04.283 (2023).

20. McKinsey. Europe's path to decarbonization McKinsey. https://www.mckinsey.com/reportlink (2020).

21. Najjar, Y. S. Hydrogen leakage sensing and control: (review). *Biomedical J. Sci. Tech. Res.* **21**(5). https://doi.org/10.26717/bjstr.2019.21.003670 (2019).

22. Nguyen, L. N. T. et al. Two decades of flask observations of atmospheric (O_2/N_2), CO_2, and APO at stations Lutjewad (the Netherlands) and Mace Head (Ireland), and 3 years from Halley station (Antarctica). *Earth Syst. Sci. Data.* **14**(2), 991–1014. https://doi.org/10.5194/essd-14-991-2022 (2022).

23. Novelli, P. C., Crotwell, A. M. & Hall, B. D. Application of gas chromatography with a pulsed discharge Helium ionization detector for measurements of molecular hydrogen in the atmosphere. *Environ. Sci. Technol.* **43**(7), 2431–2436. https://doi.org/10.1021/es803180g (2009).

24. NWP. *Werkplan Nationaal Waterstof Programma 2022–2025*. (2021).

25. Ocko, I. B. & Hamburg, S. P. Climate consequences of hydrogen emissions. *Atmos. Chem. Phys.* **22**(14), 9349–9368. https://doi.org/10.5194/acp-22-9349-2022 (2022).

26. O'Shea, S. J. et al. Area fluxes of carbon dioxide, methane, and carbon monoxide derived from airborne measurements around Greater London: a case study during summer 2012. *J. Phys. Res.* **119**(8), 4940–4952. https://doi.org/10.1002/2013JD021269 (2014).

27. Paula Pérez-Peña, M. et al. Evaluating the contribution of the unexplored photochemistry of aldehydes on the tropospheric levels of molecular hydrogen (H_2). *Atmos. Chem. Phys.* https://doi.org/10.5194/acp-2021-1052 (2022).

28. Paulot, F., Pétron, G., Crotwell, A. M. & Bertagni, M. B. Reanalysis of NOAA H2 observations: implications for the H_2 budget. https://doi.org/10.5194/egusphere-2023-1602 (2023).

29. Pétron, G. et al. Atmospheric H_2 observations from the NOAA Global Cooperative Air Sampling Network. https://doi.org/10.5194/amt-2024-4 (2024).

30. Prinn, R. G. et al. History of chemically and radiatively important atmospheric gases from the Advanced Global Atmospheric gases experiment (AGAGE). *Earth Syst. Sci. Data*. **10**(2), 985–1018. https://doi.org/10.5194/essd-10-985-2018 (2018).

31. PWC. HyWay 27: hydrogen transmission using the existing natural gas grid? Final report for the Ministry of Economic Affairs and Climate Policy. www.pwc.nl (2021).

32. Röckmann, T., Rhee, T. S. & Engel, A. Heavy hydrogen in the stratosphere. *Atmos. Chem. Phys.* **3**, 2015–2023. https://doi.org/10.5194/acp-3-2015-2003 (2003).

33. Schmidt & Seiler New method for recording molecular hydrogen in atmospheric air. *J. Geophys. Res.* **75**(9), 1713–1716. https://doi.org/10.1029/jc075i009p01713 (1970).

34. Simmonds, P. G. et al. Continuous high-frequency observations of hydrogen at the Mace Head baseline atmospheric monitoring station over the 1994–1998 period. *J. Geophys. Res. Atmos.* **105**(D10), 12105–12121. https://doi.org/10.1029/2000JD900007 (2000).

35. Sun, T., Shrestha, E., Hamburg, S. P., Kupers, R., & Ocko, I. B. Climate Impacts of Hydrogen and Methane Emissions Can Considerably Reduce the Climate Benefits across Key Hydrogen Use Cases and Time Scales. *Environ. Sci. Tech.* **58**(12), 5299–5309. https://doi.org/10.1021/acs.est.3c09030 (2024).

36. Tong, X. et al. Aircraft-based AirCore Sampling for estimates of N_2O and CH_4 emissions. *Environ. Sci. Technol.* **57**(41), 15571–15579. https://doi.org/10.1021/acs.est.3c04932 (2023).

37. Tong, X. et al. *Supporting Information (SI) for Research Article Aircraft-based AirCore sampling for estimates of N_2O and CH_4 emissions* (2023).

38. Tromp, T. K., Shia, R. L., Allen, M., Eiler, J. M. & Yung Y. L. Potential environmental impact of a hydrogen economy on the stratosphere. *Science.* **300**(5626), 1740–1742. https://www.science.org/doi/10.1126/science.1085169 (2003)

39. U.S. Department of Energy. U.S. National Clean Hydrogen Strategy and Roadmap (2022).

40. Vinković, K. et al. Evaluating the use of an unmanned aerial vehicle (UAV)-based active AirCore system to quantify methane emissions from dairy cows. *Sci. Total Environ.* **831** https://doi.org/10.1016/j.scitotenv.2022.154898 (2022).

41. Warwick, N., Griffiths, P., Keeble, J., Archibald, A. & Pyle, J. Atmospheric implications of increased Hydrogen use. https://www.gov.uk/government/publications/atmospheric-implications-of-increased-hydrogen-use (2022).

42. Warwick, N. J. et al. Atmospheric composition and climate impacts of a future hydrogen economy. *Atmos. Chem. Phys.* **23**(20), 13451–13467. https://doi.org/10.5194/acp-23-13451-2023 (2023).

43. Warwick, N. J., Bekki, S., Nisbet, E. G. & Pyle, J. A. Impact of a hydrogen economy on the stratosphere and Troposphere studied in a 2-D model. *Geophys. Res. Lett.* **31**, L05107 (2004).

44. Wentworth, W. E., Cai, H. & Stearnsb, S. Pulsed discharge Helium ionization detector Universal detector for inorganic and organic compounds at the low picogram level. *J. Chromatogr. A.* **688**, 135–152 (1994).

45. Yver, C., Schmidt, M., Bousquet, P. & Ramonet, M. Measurements of molecular hydrogen and carbon monoxide on the Trainou tall tower. *Tellus Ser. B: Chem. Phys. Meteorol.* **63**(1), 52–63. https://doi.org/10.1111/j.1600-0889.2010.00520.x (2011).

Declarations

Competing interests
The authors declare no competing interests.

Additional information
Supplementary Information The online version contains supplementary material available at https://doi.org/10.1038/s41598-024-76373-2.

Correspondence and requests for materials should be addressed to I.M.W.

Reprints and permissions information is available at www.nature.com/reprints.

Publisher's note Springer Nature remains neutral with regard to jurisdictional claims in published maps and institutional affiliations.